catalysts

MDPI

Article

Improving Fe/Al_2O_3 Catalysts for the Reverse Water-Gas Shift Reaction: On the Effect of Cs as Activity/Selectivity Promoter

Laura Pastor-Pérez [1,2,*], Mihir Shah [1], Estelle le Saché [1] and Tomas Ramirez Reina [1,*]

[1] Department of Chemical and Process Engineering, University of Surrey, Guildford GU2 7XH, UK; ms00440@surrey.ac.uk (M.S.); e.lesache@surrey.ac.uk (E.l.S.)

[2] Laboratorio de Materiales Avanzados, Departamento de Química Inorgánica Instituto Universitario de Materiales de Alicante Universidad de Alicante, Apartado 99, E03080 Alicante, Spain

* Correspondence: l.pastorperez@surrey.ac.uk (L.P.-P.); t.ramirezreina@surrey.ac.uk (T.R.R.); Tel.: +34-96-590-9350 (L.P.-P.); +44-148-368-6597 (T.R.R.)

Received: 14 November 2018; Accepted: 26 November 2018; Published: 3 December 2018

Abstract: The conversion of CO_2 into CO via the Reverse Water–Gas Shift (RWGS) reaction is a suitable route for CO_2 valorisation. Fe-based catalysts are highly active for this reaction, but their activity and selectivity can be substantially boosted by adding Cs as a promoter. In this work we demonstrate that Cs modifies the redox behaviour and the surface chemistry of the iron-based materials. The metallic dispersion and the amount of metallic Fe centres available for the reaction depends on Cs loading. 5 wt. % of Cs is an optimum amount of dopant to achieve a fair activity/selective balance. Nevertheless, depending on the RWGS reactor operational temperature, lower concentrations of Cs also lead to acceptable catalytic performance. Along with the excellent activity of the prepared materials this work showcases their robustness for long-term runs and the strong impact of H_2/CO ratio in the overall catalytic performance.

Keywords: RWGS; Fe catalysts; Caesium promoter; CO_2 conversion

1. Introduction

Some of the most severe issues facing society today include anthropogenic induced climate change and ocean acidification. Atmospheric CO_2 is rising year on year and global average temperatures have risen in parallel. In 2018 the concentrations of CO_2 in the atmosphere passed 410 parts per million for the first time in several million years [1], and became the hottest year since records began. One method for reducing CO_2 emissions and mitigating the associated climate change is to capture anthropogenic emissions and store it in geological formations, such as depleted gas reservoirs [2]. Alternatively, CO_2 can be converted into value-added fuels or chemicals such as methanol.

Currently however, global demand for chemicals derived from sequestered CO_2 fails to contribute significantly to help meet global carbon reduction targets; CO_2 consumption by catalytic conversion is equivalent to only 0.5% of the total global CO_2 emissions [3]. The limited adoption of carbon capture and utilisation in industry is partially due to the thermodynamic stability of CO_2. Because of its stability, it is relatively unreactive and therefore its conversion is energy intensive. Furthermore, many of the methods for CO_2 valorisation require hydrogen as a feedstock and finding a carbon neutral and cost effective hydrogen source is not always straightforward [4]. In any case, the development of an economically viable CO_2 conversion process is key to achieving a circular economy pathway.

At present, the Fischer Tropsch (FT) process, which produces synthetic liquid hydrocarbon fuels, as well as the CAMERE process, which produces methanol, have both been examined extensively

due to their viability for CO_2 conversion on a large scale [5–7]. Both reactions can be carried out in conjunction with the Reverse Water–Gas Shift (RWGS) reaction, which converts CO_2 and H_2 into CO and H_2O.

Because of its endothermic nature, RWGS is thermodynamically favourable at high temperatures as shown in Equation (1). At lower temperatures, the equilibrium will increasingly favour the water-gas shift reaction—WGS (reverse of Equation (1)) and methanation (Equation (2)) reactions, given their exothermic nature. Due to the stoichiometry of the reaction, altering pressure has no significant effect on the reaction activity or the position of the equilibrium [8,9].

$$H_2 + CO_2 \rightleftharpoons CO + H_2O \ \Delta H^{\circ}_{298k} = 41.2 \text{ kJ·mol}^{-1}, \quad (1)$$

$$CO_2 + 4H_2 \rightleftharpoons CH_4 + 2H_2O \ \Delta H^{\circ}_{298k} = -165 \text{ kJ·mol}^{-1}, \quad (2)$$

In recent years, numerous studies have been dedicated to improving the catalytic performance of the RWGS reaction, with considerable attention on monometallic catalysts such as Pt [10] and Cu [11], bimetallic catalysts such as Cu–Ni [12], and transition metal carbide catalysts, such as Mo_2C [13]. Among the wide variety of catalysts reviewed in literature, iron-based catalysts have shown the greatest potential, due to their thermal stability and high oxygen mobility [14,15], while remaining a credible option in terms of costs of manufacture [16]. Transition metal oxides, such as TiO_2 [17], CeO_2 [18], and Al_2O_3 [19], have been investigated as supports for catalysts used in the RWGS reaction. The transition metal oxides support helps with dispersion of the active phase due to their large surface area. Additionally, reducible oxides boost oxygen mobility which in turns prevents coking [20]. In addition to the support, the active phase can also be promoted by adding an alkali metal [21]. Indeed the addition of alkali metals has repeatedly shown to improve CO_2 adsorption, as the presence of these species significantly modifies the electronic density of the catalyst's surface as well as improves the dispersion of the active phase [22,23]. Previous reports in literature pointed out that the valence s-orbital of the alkali metal hybridises with the valence band of the active metal, allowing the alkali metal to easily donate electrons, consequently enhancing the catalyst basicity [24].

Among the alkaline metals, potassium has been the most extensively studied as a catalytic promoter, often in conjunction with iron [25,26]. Caesium, on the other hand, has been subject to far fewer studies in the field. A recent work of our team revealed that Cs promoters can improve conversion and selectivity compared to un-promoted Fe/Cu-based catalysts [27]. Furthermore, the study also highlighted that Cs is more prone to donate electrons due to its larger ionic radius compared to potassium, implying that a Cs-promoted catalyst could be better at adsorbing CO_2 compared to a K-promoted catalyst.

While it is understood why the addition of an alkali metal promoter would improve CO_2 adsorption, a study by Yang et al., which tested K-doped Pt/zeolites for the RWGS reaction, has shown that while increasing the K loading initially improves CO_2 conversion in the RWGS, after the K/Pt atomic ratio exceeded 80, the CO_2 conversion decreased [28]. A study on CO_2 conversion to propanol by Ahlers et al. which tested Cs-doped Au/TiO_2, showed that there is a maximum effect on propanol selectivity between 4–7% of Cs and such a positive effect disappears for the catalysts with Cs loading above 7 wt. % [29]. A similar question arises for the RWGS—what is the effect of Cs loading as a promoter, and is there a threshold in terms of activity/selectivity improvement.

Under these premises, this study investigates the effect of Cs loading on a Fe_2O_3/Al_2O_3 catalyst for CO_2 valorisation via reverse water-gas shift. The different weight loadings (1, 2.5, and 5 wt. %) help elucidate the impact of Cs on the catalytic performance and the characterisation study by means of XPS, XRD, BET, and H_2-TPR is useful to correlate the catalytic trends with the structural and electronic properties of the different catalysts.

2. Results and Discussion

2.1. Textural Properties

The N_2 adsorption-desorption isotherms of the calcined samples are presented in Figure 1. All samples are mesoporous materials presenting a type IV isotherm according to IUPAC classifications, also indicating multilayer adsorption. The textural properties of the catalysts are governed by the primary support (γ-Al_2O_3).

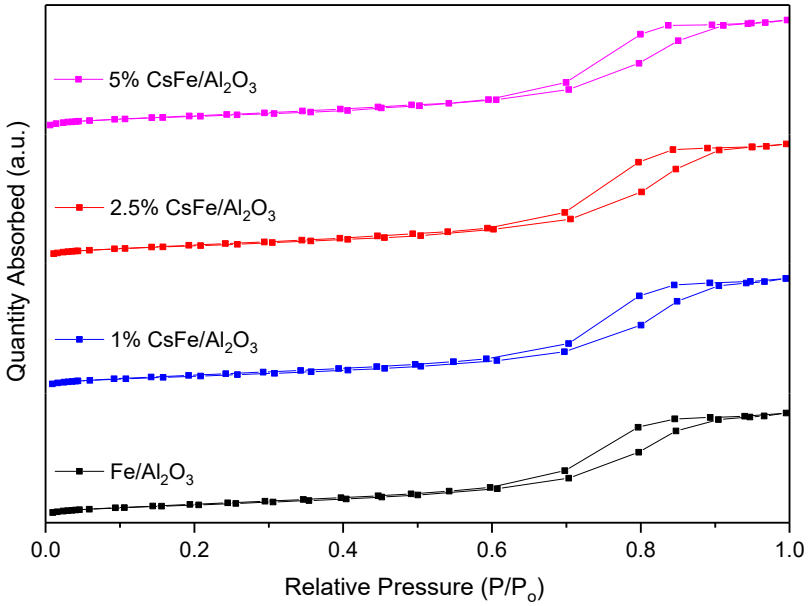

Figure 1. N_2 adsorption-desorption isotherms of the calcined samples.

Table 1 lists the surface area, pore volume, and average pore diameter of each catalyst after calcination. The addition of a caesium promoter has a noticeable effect on the specific surface area and pore volume. With each increase in caesium loading, the surface area decreases, with the 5% $CsFe/Al_2O_3$ sample exhibiting a value of 149 m^2/g compared to Fe/Al_2O_3, which has a surface area of 174 m^2/g. The reduction of surface area and total pore volume are in good agreement with previous observations in literature [29], and indicates that Cs species could be partially covering the mesopores of the alumina support.

Table 1. Textural Properties of the prepared catalysts.

Catalyst	Surface Area (m^2/g)	Pore Volume (cm^3/g)	Pore Diameter (nm)
Fe/Al_2O_3	174	0.470	8.73
1% $CsFe/Al_2O_3$	168	0.467	8.83
2.5% $CsFe/Al_2O_3$	153	0.421	8.75
5% $CsFe/Al_2O_3$	149	0.401	8.83

2.2. XRD

The XRD profiles in Figure 2 reveal the crystalline structure of the calcined catalysts. The samples are composed of small peaks of hematite α-Fe_2O_3 structure (JCPDS#-24-0072) at $2\theta = 33.1°$, 35.6°, 49.4°, 54.0°, 62.4°, 64.0°, and face-centred cubic crystal structure of ferrite Fe_3O_4 (JCPDS#-19-0629) at $2\theta = 30.0°$, 35.4°, 56.9°, 62.5°. This reveals that iron oxide has been through different oxidation states. Overall the peaks ascribed to iron crystalline phases are very small and hard to detect indicating a good dispersion of the iron oxide phase over the commercial alumina support. Some typical reflexions attributed to the primary support γ-Al_2O_3 (JCPDS# 00-048-0367) are identified by assigning peaks at

2θ = 37.6°, 45.8°, 67°. No peaks relating to Cs_2O are observed, suggesting that the Cs-particles are small and dispersed over the support corroborating the successful catalysts preparation.

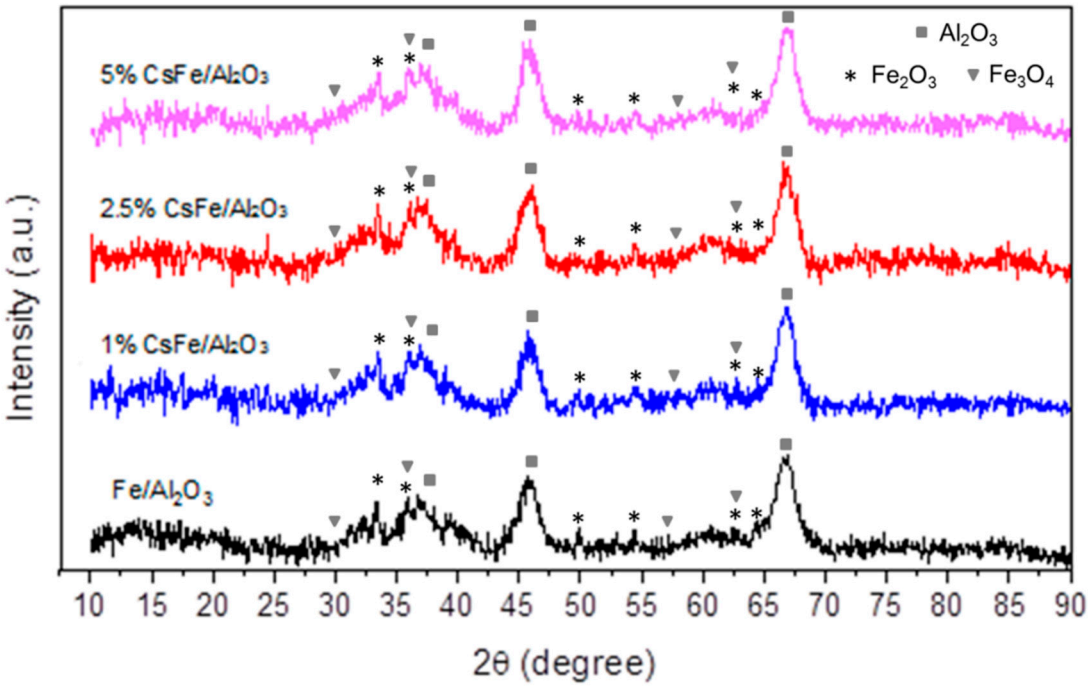

Figure 2. X-ray diffraction profiles of the calcined samples.

2.3. H_2-TPR

Assessing the redox properties of the catalysts, as well as interactions between the support and metallic species, is of great importance for hydrogenation reactions like RWGS. The reducibility of the catalysts was assessed by H_2-TPR studies, the profiles of which are shown in Figure 3.

All catalyst profiles present two reduction zones, which can be attributed to the reduction of the iron oxides, which occur over two separate stages. The first and larger zone, which has a range of 290–520 °C, is the first stage of the overall reduction, whereupon Fe_2O_3 was reduced to Fe_3O_4. The second zone, with a range of 580–800 °C, corresponds to the reduction of Fe_3O_4 to Fe through FeO as previously reported elsewhere [30].

H_2-TPR can also help to elucidate the influence of the promoter on the reducibility of a specific compound in a catalyst. A remarkable shift of both peaks towards lower temperatures was observed with the addition of 1% of caesium, indicating that Cs improves the overall reducibility. Cs basic character eases electron transfer from Cs to FeO_x, facilitating iron phases reduction at lower temperatures. Further increments on Cs loading (2.5 and 5%) do not have a remarkable effect on the overall reducibility of the catalysts and although the reduction zones are shifted to lower temperatures upon increasing Cs loading, it seems that 1% is enough to alter significantly the redox behaviour.

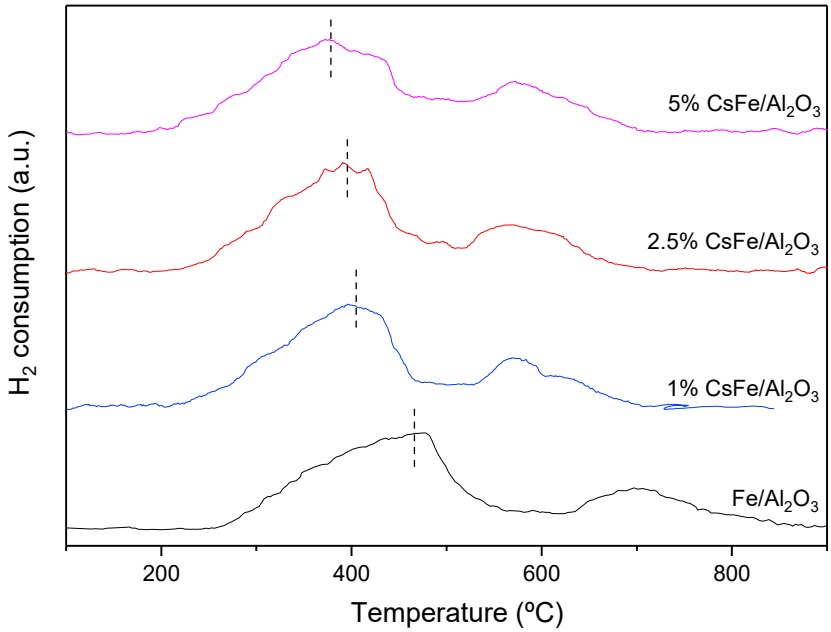

Figure 3. TPR profiles of the calcined samples.

2.4. XPS

The Fe $2p_{3/2}$ and Cs $3d_{5/2}$ spectra of the reduced samples are represented in Figure 4 with the main peaks summarised in Table 2. It can be observed on the Fe $2p_{3/2}$ spectra that after the reduction at 800 °C, only a small fraction of the iron species was in the metallic state and that different iron species, such as Fe_2O_3 and Fe_3O_4, co-exist in the surface of the reduced catalysts. The Fe $2p_{3/2}$ binding energies (BE) peaks around ~706 eV are characteristic of metallic Fe, while the bands around 708.6–709.8 and 710.9–711.9 correspond to Fe^{2+} and Fe^{3+}, respectively [31]. From Table 2, it is clear that increasing the Cs loading increases the Fe metallic content in the surface, with the 5% $CsFe/Al_2O_3$ sample having the highest amount of metallic Fe. An interesting effect is observed in terms of $Fe^{3+}/Fe^{2+}/Fe$ proportions. For low Cs loadings, the reduction of Fe^{3+} to Fe^{2+} seems to be favoured and the Fe^0 remains constant. In other words, low Cs loading seems to stabilise FeO species in the surface. However, higher Cs concentrations (5%) seem to favour the complete reduction of Fe^{3+} to Fe^0 since this sample presents the greater proportion of metallic iron in the surface, avoiding the stabilisation of Fe^{2+} species. This effect is also corroborated by the Fe/Al ratios depicted in Table 2. For low Cs loadings there is less Fe exposed in the surface, probably due to the partial coverage of these species by Cs, while for the 5% sample the amount of iron exposed in the surface increases, likely due to the presence of exposed metallic iron clusters re-dispersed upon intimate interaction with Cs.

It is important to note that the reducibility of FeO_x increases heavily upon addition of Cs, in good agreement with the TPR data. In fact, the total metallic iron on the surface goes from 4% in the non-promoted material to 20% in the 5% Cs doped catalysts. It is the clear that Fe in the Cs-doped catalyst is electronically richer compared to the reference system. This is a very relevant result and reflects how Cs tunes the surface chemistry of the Fe based catalysts. The electronic enrichment also implies that the Cs-doped Fe/Al_2O_3, especially the 5% $FeCs/Al_2O_3$ sample, should be more prone to interact and activate CO_2.

Table 2. Binding energies of the Fe $2p_{3/2}$ and Ce $3d_{5/2}$ levels for the pre-reduced catalysts and Fe/Al atomic ratios.

Catalysts	Fe $2p_{3/2}$ (eV)			Cs $3d_{5/2}$ (eV)	Fe_{total}/Al (at/at)	Cs/Fe
	Fe^{3+}	Fe^{2+}	Fe	Cs^{1+}		
5% $CsFe/Al_2O_3$	710.9 (62%)	708.6 (18%)	706.7 (20%)	723.7–725.9	0.077	0.708
2.5% $CsFe/Al_2O_3$	711.5 (25%)	709.5 (63%)	706.7 (14%)	725.5	0.048	0.460
1% $CsFe/Al_2O_3$	711.9 (34%)	709.8 (52%)	706.5 (13%)	724.5	0.059	0.202
Fe-Al_2O_3	712.8 (43%)	710.3 (53%)	706.5 (4%)	-	0.077	-

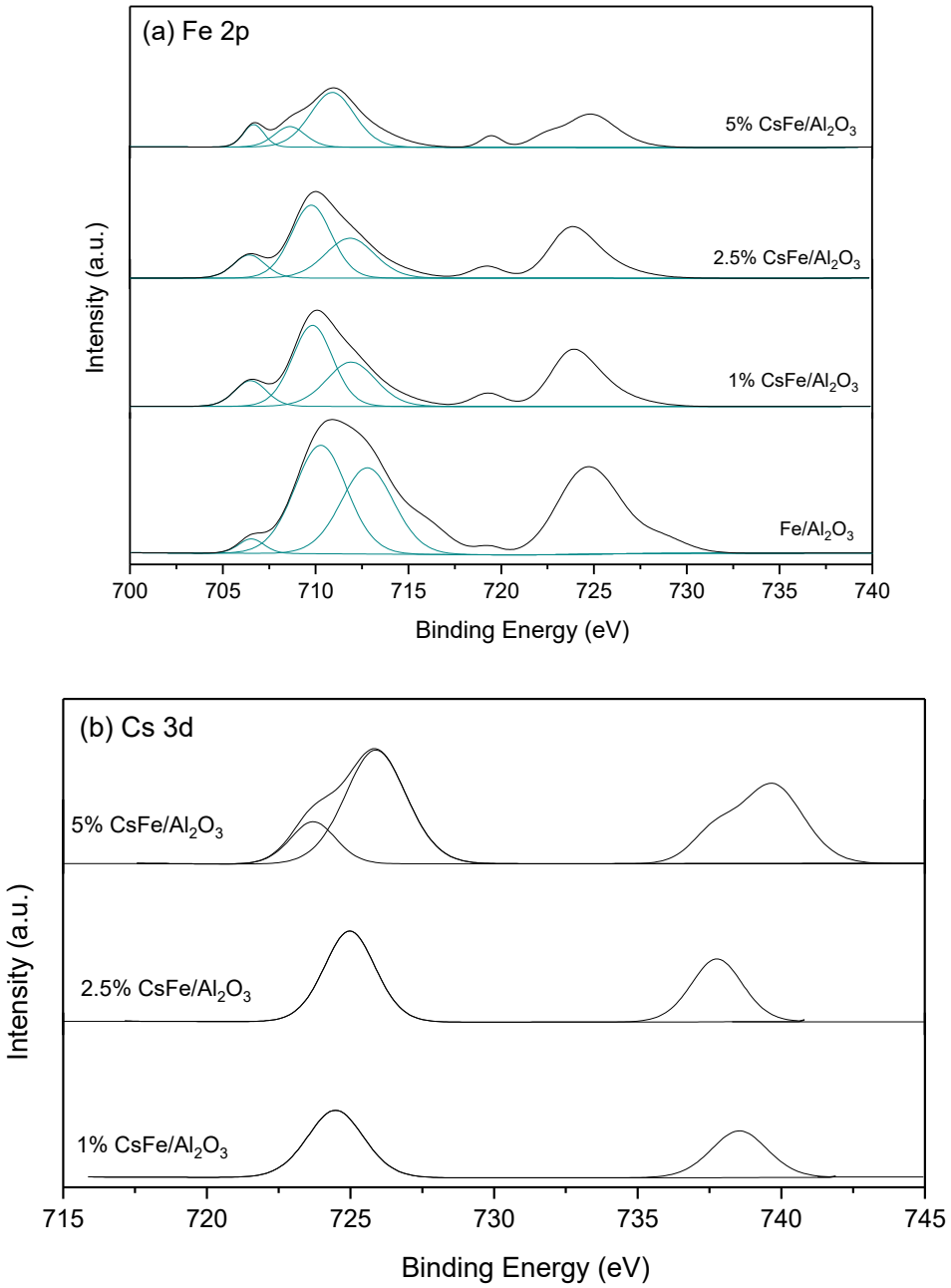

Figure 4. XPS core level of (**a**) Fe 2p and (**b**) Cs3d spectra.

As for the chemical nature of caesium species on the surface, Figure 4b depicts the XPS spectra. Overall for Cs-based samples the peak identification is relatively difficult and there is some debate in literature. For the samples with 1 and 2.5% of Cs the binding energy of the Cs $3d_{5/2}$ photoelectron

around 724.5–725.6 can be ascribed to Cs in contact with FeO_x oxides or Cs_xO_y species. The shift to higher B.E. for the 2.5% Cs-doped sample could be due to the surface enrichment of Fe^{2+} and metallic Fe and the interaction of these species with Cs. As reported in NIST database, the close contact between Cs and metallic Fe shifts the binding energy towards higher values [32]. Interestingly, the deconvolution of Cs $3d_{5/2}$ spectra of 5% caesium-doped catalyst showed two peaks at 723.7 and 726.5 eV. Herein, the shifts to higher values are more notorious (726.5 eV) and it could be related with the higher amount of Fe metallics in this sample. Furthermore, the presence of a secondary peak at 723.7 eV can be assigned to Cs^+, a more electropositive species [32].

2.5. Catalytic Behaviour

2.5.1. Effect of the Promoter on Catalytic Performance

Once the structural and electronic properties of the catalysts had been analysed, the synthesised catalysts were tested in the RWGS reaction. The catalytic activities in terms of CO_2 conversion of the prepared samples are shown in Figure 5.

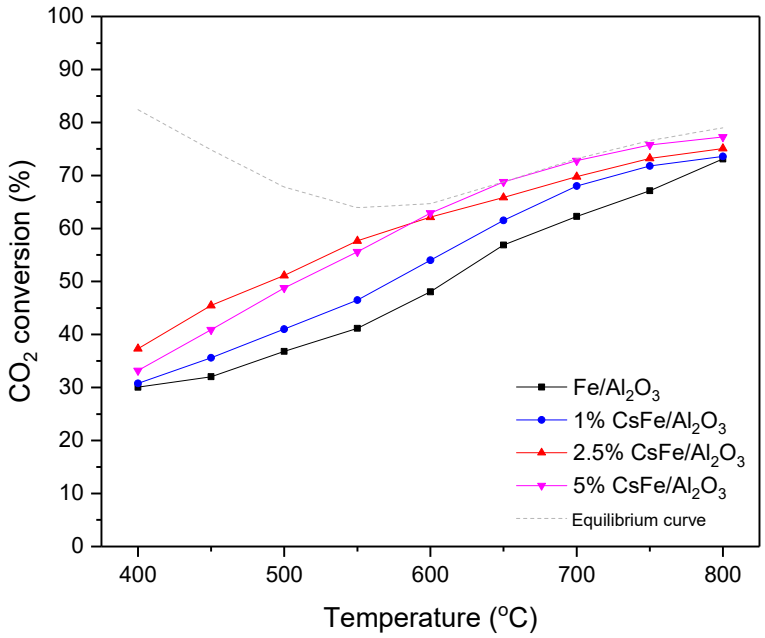

Figure 5. CO_2 Conversion at 400–800 °C, WHSV of 12,000 mL/g_{cat}h, and H_2/CO_2 ratio of 4:1.

There is a clear effect of the temperature of the RWGS—conversion steadily increases with temperature reflecting the endothermic nature of the reaction. Interestingly, at lower temperatures (400 °C–600 °C), 2.5% $CsFe/Al_2O_3$ displayed the highest level of conversion, whilst at higher temperatures (600 °C–800 °C), 5% $CsFe/Al_2O_3$ exhibited the best conversion levels. In all the studied temperature ranges, the reference Fe/Al_2O_3 showed the lowest CO_2 conversion, with 1% $CsFe/Al_2O_3$ having slightly higher CO_2 conversion.

It could be anticipated that the 5% $CsFe/Al_2O_3$ catalyst would have the highest conversion throughout; the catalyst presented the best reducibility (as discussed in the TPR section) and a higher amount of metallic Fe, favouring the CO_2 adsorption. This catalyst also presents a better Fe dispersion on the surface compared to that of the 2.5% $CsFe/Al_2O_3$, which explains its superior activity in the medium–high temperature range. The study by Yang et al. found that when loading of the alkali metal promoter becomes too great, the promoter can fail to disperse uniformly, leading to an uneven distribution of the active phase. However, the XRD profile (Figure 2) and XPS Fe/Al ratio (Table 2) show that caesium and iron were evenly distributed for all catalysts, even for relatively high Cs loadings (5% $CsFe/Al_2O_3$), providing suitable availability of active phases.

Although the 5% Cs loading seems to be the best performing catalyst, if the RWGS reaction is integrated with Fischer-Tropsch process, as proposed by Pastor-Pérez et al. [27], the 2.5% $CsFe/Al_2O_3$ catalyst would be the most logical choice, based solely on CO_2 conversion. Indeed, as the Fischer-Tropsch process takes place at low temperatures, running the RWGS reactor at temperatures below 600 °C could facilitate heat and energy integration. However, if the RWGS reaction is integrated with methanol production via the CAMERE process, the 5% $CsFe/Al_2O_3$ catalyst would be most logical choice, as the CAMERE process is conducted at higher temperatures [33].

Along with conversion, selectivity is a key factor when assessing catalytic performance for RWGS, especially at low temperature, due to the strong competition with CO_2 methanation which consumes a significantly larger amount of hydrogen [34]. For all catalysts, the selectivity of CO increases with temperature, while CH_4 selectivity shows the opposite trend. In terms of CO selectivity, the catalyst performances were ranked as: 5% $CsFe/Al_2O_3$ > Fe/Al_2O_3 > 2.5% $CsFe/Al_2O_3$ > 1% $CsFe/Al_2O_3$. The excellent selectivity of the 5% $CsFe/Al_2O_3$ sample could be attributed to the boosted electronic effects of Cs on Fe. As revealed in the XPS study, the amount of metallic Fe is higher for this sample, indicating a higher charge transfer from Cs to Fe. Lower CO selectivities were obtained for the 1% and 2.5% $CsFe/Al_2O_3$ samples compared to the non-doped sample, which could be attributed to the lower Fe dispersion obtained with these samples (see Fe/Al ratios on Table 2), despite their larger content of metallic iron on the surface.

In terms of CH_4 selectivity, the catalyst performances were ranked as: Fe/Al_2O_3 > 1% $FeCs/Al_2O_3$ > 2.5% $FeCs/Al_2O_3$ > 5% $FeCs/Al_2O_3$. The results from Figure 6 indicate that the caesium promoter inhibits the methanation reaction at lower temperatures, and that the greater amount of caesium the stronger the inhibition of CH_4 production is achieved. The result of an alkali metal promoter suppressing methanation is in good agreement with previous observations in literature [10,35], highlighting that the alkali metal potassium weakens the CO adsorption catalyst's surface. The weakened adsorption hinders further hydrogenation of CO into CH_4 via C–O bond dissociation.

In summary, we identified 5% loading of Cs as the best choice in this study. In fact there are no significant benefits in terms of CO_2 conversion when 5% Cs is compared to 2.5%, but there is a remarkable gain in selectivity. Indeed, the 5% Cs loaded catalyst barely forms methane even at the low temperature range. Therefore, the 5% Cs loaded sample was selected for further catalytic studies, such as the effect of H_2/CO_2 ratio and the stability test.

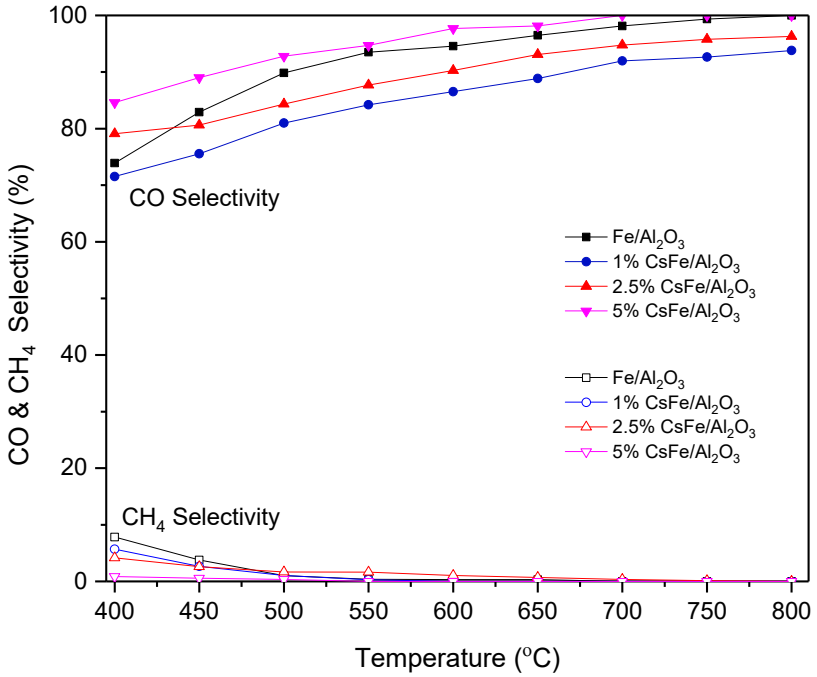

Figure 6. CO and CH_4 Selectivity at 400–800 °C, WHSV of 12,000 mL/g_{cat}h, and H_2/CO_2 ratio of 4:1.

2.5.2. Effect of H_2:CO_2 Ratio on Catalytic Performance

A major concern of adapting RWGS for industrial applications is obtaining a sustainable and cheap source of hydrogen. This so-called renewable hydrogen is typically produced by electrolysis, however in recent times, alternative hydrogen sources have been investigated, such as using cyanobacteria, biomass, microbial electrolysis, and solar energy [4]. Despite investigation into new sources, hydrogen remains expensive and poses a significant barrier to the implementation of the RWGS for practical applications.

Given its high cost, the catalytic performance tests were repeated with H_2/CO_2 ratio being altered to observe the impact that decreasing the ratio would have. While it was expected that reducing the H_2/CO_2 ratio would decrease CO_2 conversion [25,36], if the decrease in conversion is relatively small and the profitability of the process remained the same or increased, then it could be recommended to use a lower H_2/CO_2 ratio for the RWGS reaction.

For the test to measure the effect of H_2/CO_2 ratio on the catalytic performance, the H_2/CO_2 ratio was varied from 4:1 to 1:1 using the 5% $FeCs/Al_2O_3$ sample (Figure 7). Between 400–450 °C, CO_2 conversion is similar between the H_2/CO_2 ratios, with conversion around 35–40% for both 4:1 and 1:1 ratio at 400 °C. However, at 500 °C a difference in CO_2 conversion between the ratios begins to arise, with a difference of 11% between the 4:1 and 1:1 H_2/CO_2 ratios. At 800 °C, the difference in conversion widened, with a difference of 21% between the different H_2/CO_2 ratios. While the difference in conversion increases with temperature, the opposite is true with CO selectivity. At 450 °C, the difference in CO selectivity between the ratios was 38%, while at 800 °C, the difference in selectivity had fallen to only 9%.

If the RWGS is to be integrated with the Fischer-Tropsch process, then the 1:1 H_2/CO_2 ratio would be suitable, based solely on CO_2 conversion results. However, the poor CO selectivity at low temperatures limits the appeal of using the 1:1 ratio, and it would be necessary to use a hydrogen rich stream with H_2/CO_2 ratio around 4 to maximise both activity and selectivity.

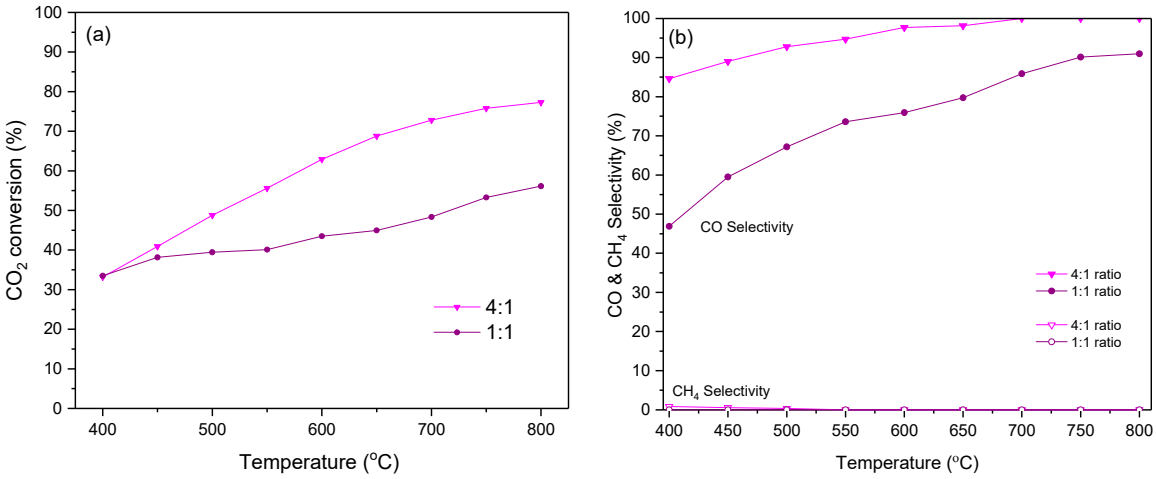

Figure 7. (**a**) CO_2 Conversion and (**b**) CO and CH_4 selectivity at 400–800 °C, WHSV of 12,000 mL/g_{cat}h, and various H_2/CO_2 ratios using 5% $CsFe/Al_2O_3$.

2.5.3. Stability Test

CO_2 valorisation technology may require continuous operation, for instance if the CO_2 conversion unit is meant to deal with continuous emissions of flue gases in a heavy carbon industry. For example, at a power plant, converting CO_2 exhausted in flue gas into CO would be an ongoing process, and therefore the long-term stability of the catalyst would be vital. For the stability test, the reaction conditions were sufficiently far from equilibrium, with temperature held at 550 °C, and tested for 40 h (WHSV of 12,000 mL/g_{cat}h with a H_2/CO_2 ratio of 4:1). From Figure 8, the catalyst maintained

stability after 40 h, with CO_2 conversion remaining approximately constant at 57%. It is interesting to note that there is a slight induction period at the initial stages of the stability test with smooth increase of the conversion which may indicate an "in-situ" activation of catalysts, perhaps due to active phase re-dispersion. Overall, the promising performance of the 5% $CsFe/Al_2O_3$ catalyst in terms of stability can be linked to its robustness to sintering and carbon deposition resistance provided by Cs as a dopant, as previously demonstrated by our group [27].

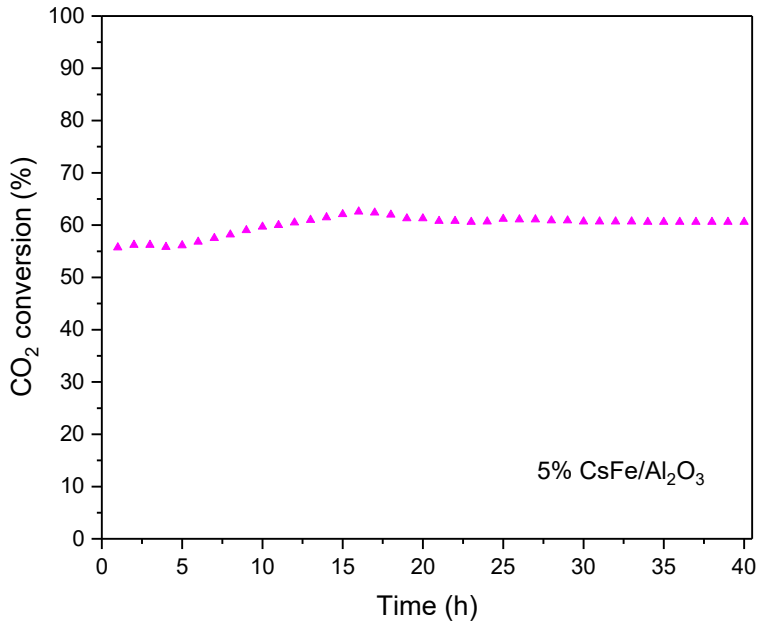

Figure 8. Stability test for CO_2 Conversion at 550 °C, WHSV of 12,000 mL/g_{cat}h, and H_2/CO_2 ratio of 4:1.

3. Materials and Methods

3.1. Catalyst Synthesis

The catalysts were synthesised by sequential wet impregnation. The necessary amount of Fe $(NO_3)_2 \cdot 9H_2O$ (Sigma-Aldrich, St. Louis, MO, USA, 99.95%) to obtain 15 wt.% Fe_2O_3 was dissolved in acetone. The Puralox SCFa-230 γ-alumina powder (Sasol, Johannesburg, South Africa, ≥99%) was then impregnated with the solution containing the metallic precursor for 4 h in a rotavapor. The solvent was removed by evaporation at reduced pressure in the rotavapor and the resultant slurry was dried at 100 °C overnight and calcined at 750 °C for 4 h.

The resultant Fe/Al_2O_3 (oxygen is Fe formulation is omitted for sake of simplicity) was divided equally, with each batch designated different loadings of Cs from 0% to 5% wt.%. For each batch, the mass of Cs_2CO_3 precursor (Sigma-Aldrich, ≥99%) was determined and dissolved in ethanol. Fe/Al_2O_3 was then impregnated for 4 h in the rotavapor with the solution containing the Cs_2CO_3 precursor. The solvent was removed by evaporation at reduced pressure and the resultant slurry was dried at 100 °C overnight and calcined at 750 °C for 4 h. The resulting catalyst produced were Fe/Al_2O_3, 1% $FeCs/Al_2O_3$, 2.5% $FeCs/Al_2O_3$, and 5% $FeCs/Al_2O_3$, where the percentage denotes the weight loading of Cs in the catalyst.

3.2. Catalyst Characterisation

X-ray diffraction (XRD) analysis was conducted on fresh and spent catalysts using an X'Pert Powder diffractometer from PANalytical (Royston, United Kingdom) at room temperature, using the powder method. Diffraction patterns were recorded at 45 kV and 40 mA, using Cu Kα radiation

(λ = 0.154 nm). The 2θ angle was increased by a step size of 0.05° every 450 s over a scanning range of 10–90°.

The elemental composition was determined via means of X-ray fluorescence (XRF), which was conducted on an EDAX Eagle III spectrophotometer (Mahwah, NJ, USA) with a rhodium source of radiation (at 40 kV).

The textural properties of catalysts were determined from N_2 adsorption–desorption isotherms recorded on a Micrometrics TriStar II 3020 apparatus (Norcross, GA, USA) at the boiling point of nitrogen (77 K). Prior to the adsorption–desorption measurements, the samples were degassed at 250 °C for 2 h in a vacuum. The specific surface area was determined using the Brunauer–Emmett–Teller (BET) method, whilst average pore size and pore volume were obtained by the Barret–Joyner–Halenda (BJH) method.

Temperature programmed reduction with H_2 (H_2-TPR) was conducted in a conventional U-shaped quartz reactor, using a gaseous mixture of 5% H_2/He and flow rate of 50 mL/min, with a heating rate of 10 °C/min. Prior to the TPR runs, the catalyst was pre-treated with He (50 mL/min) at 150 °C for 1 h.

XPS measurements were performed with a K-ALPHA spectrometer (Thermo Fisher Scientific, Waltham, MA, USA) operated in the constant energy mode with survey scan pass energies of 200 eV and narrow scan energies of 50 eV, to measure the whole energy band as well as selectively measure particular elements. All XPS spectra were acquired using Al-Kα radiation (1486.6 eV) with a twin crystal monochromator, yielding a focused X-ray spot (elliptical in shape with a major axis length of 400 μm) at 3 mA $\times$ 12 kV. Charge compensation was attained with the system flood gun, which provides low energy electrons and low energy argon ions from a single source. For the reference binding energy, the C1s core level was used, located at 284.6 eV. All samples were reduced ex-situ at 800 °C, and before recording the spectrum, the samples were maintained in the analysis chamber until a residual pressure of ca. 5×10^{-7} N/m^2 was reached.

3.3. Catalytic Tests

The behaviour of the studied catalysts was evaluated in a vertical fixed-bed quartz reactor (10 mm ID), at atmospheric pressure, with the product stream monitored by an on-line gas analyser (ABB AO2020 Advanced Optima Process Gas Analyser, ABB, Mannheim, Germany). 250 mg of catalyst was used for each test, supported by a bed of quartz wool centrally positioned in the reactor. Prior to each reaction, the catalysts were reduced for 1 h in situ under a total gas flow of 100 mL/min, composed of 10% H_2 carried by N_2 at 800 °C.

All tests were conducted at a constant weight hourly space velocity (WHSV) of 12000 mL/g_{cat}h with H_2/CO_2 ratio of 4:1 or 1:1 balanced in N_2. The temperature range of the tests was 400 to 800 °C, increased in 50 °C increments, with a heating rate of 10 °C/min. The effluent compositions were documented for each temperature interval once the reaction had reached steady-state. The stability test was conducted for 36 h at 550 °C with a H_2/CO_2 ratio of 4:1. The conversions and selectivities were calculated as follows:

$$\text{CO}_2 \text{ conversion } (\%) = \frac{[\text{CO}_2]_{\text{In}} - [\text{CO}_2]_{\text{Out}}}{[\text{CO}_2]_{\text{In}}} \times 100, \quad (3)$$

$$\text{CO selectivity } (\%) = ([\text{CO}]_{\text{Out}})/([\text{CO}_2]_{\text{In}} - [\text{CO}_2]_{\text{Out}}) \times 100, \quad (4)$$

$$\text{CH}_4 \text{ selectivity } (\%) = ([\text{CH}_4]_{\text{In}})/([\text{CO}_2]_{\text{In}} - [\text{CO}_2]_{\text{Out}}) \times 100, \quad (5)$$

where $[CO_2]_{In}$ and $[CO_2]_{Out}$ are CO_2 inlet and outlet mole concentrations respectively, $[CH_4]_{Out}$ is the CO outlet mole concentration, and $[CH_4]_{Out}$ is the methane outlet mole concentration.

4. Conclusions

Highly effective multicomponent iron-based catalysts for CO_2 valorisation via RWGS have been developed in this study. All of the catalysts tested were highly active, with high conversion and CO selectivity. However, this study reveals that the reference catalyst Fe/Al_2O_3 can be remarkably promoted by the addition of Cs, with the 5% $FeCs/Al_2O_3$ exhibiting the best CO selectivity and lowest CH_4 selectivity. The 2.5% $FeCs/Al_2O_3$ catalyst had the best CO_2 conversion at low temperatures, while the 5% $FeCs/Al_2O_3$ catalyst had the best CO_2 conversion at high temperatures.

The excellent CO_2 conversion of the 5% $FeCs/Al_2O_3$ at medium-high temperatures can be attributed to the fact that increasing the Cs loading improves the overall reducibility of the catalyst. The presence of Cs improves CO_2 activation by facilitating the CO_2 adsorption by easing electron transfer from the catalyst to the reactive species. In addition, the high CO selectivity of 5% $FeCs/Al_2O_3$ can be ascribed by Cs suppressing the formation of CH_4, very likely by weakening the strength of the CO adsorption on the catalyst surface and avoiding its hydrogenation to methane. However, the better CO_2 conversion of the 2.5% $FeCs/Al_2O_3$ at low temperatures indicates that too much Cs can have a counterproductive effect. Therefore, the amount of dopant and overall catalyst choice (i.e., 2.5% of Cs vs. 5%) will strongly depend on the operation conditions of the shift reactor.

The strong effect of the H_2/CO_2 ratio highlighted the need of a H_2-rich stream to achieve high levels of activity and selectivity in the RWGS reaction. Finally, our Cs-doped catalysts presented excellent stability for long-term runs, with remarkable selectivity towards CO production while operating at relatively high space velocities indicating their suitability to be further explored for their utilisation in compact CO_2 conversion reactors.

Author Contributions: Methodology, L.P.-P. and E.l.S.; formal analysis, L.P.-P.; investigation, M.S. and E.l.S.; writing—original draft preparation, M.S.; writing—review and editing, L.P.-P.; supervision, T.R.R.; funding acquisition, T.R.R.

Funding: This research was funded by the Department of Chemical and Process Engineering at the University of Surrey and by the EPSRC, grant EP/R512904/1, as well as the Royal Society, Research Grant RSGR1180353. LPP acknowledge Comunitat Valenciana for her APOSTD2017 fellowship. This work was also partially sponsored by the CO_2 Chem through the EPSRC grant EP/P026435/1.

Acknowledgments: The authors acknowledge Sasol for supplying the alumina.

Conflicts of Interest: The authors declare no conflict of interest. The funders had no role in the design of the study; in the collection, analyses, or interpretation of data; in the writing of the manuscript, or in the decision to publish the results.

References

1. Nooa Research. Available online: https://research.noaa.gov/article/ArtMID/587/ArticleID/2362/Another-climate-milestone-falls-at-NOAA%E2%80%99s-Mauna-Loa-observatory (accessed on 7 November 2018).
2. Cuéllar-Franca, R.M.; Azapagic, A. Carbon capture, storage and utilisation technologies: A critical analysis and comparison of their life cycle environmental impacts. *J. CO_2 Util.* **2015**, *9*, 82–102. [CrossRef]
3. Olivier, J.G.J.; Schure, K.M.; Peters, J.A.H.W. *Trends in Global CO_2 and Total Greenhouse Gas Emissions: 2017 Report*; PBL Netherlands Environmental Assessment Agency: The Hague, The Netherlands, 2017.
4. Centi, G.; Quadrelli, E.A.; Perathoner, S. Catalysis for CO_2 conversion: A key technology for rapid introduction of renewable energy in the value chain of chemical industries. *Energy Environ. Sci.* **2013**, *6*, 1711–1731. [CrossRef]
5. Jahangiri, H.; Bennett, J.; Mahjoubi, P.; Wilson, K.; Gu, S. A review of advanced catalyst development for fischer-tropsch synthesis of hydrocarbons from biomass derived syn-gas. *Catal. Sci. Technol.* **2014**, *4*, 2210–2229. [CrossRef]
6. Joo, O.-S.; Jung, K.-D.; Yonsoo, J. Camere process for methanol synthesis from CO_2 hydrogenation. In *Studies in Surface Science and Catalysis*; Park, S.-E., Chang, J.-S., Lee, K.-W., Eds.; Elsevier: Amsterdam, The Netherlands, 2004; Volume 153, pp. 67–72.
7. Samimi, F.; Rahimpour, M.R.; Shariati, A. Development of an Efficient Methanol Production Process for Direct CO_2 Hydrogenation over a $Cu/ZnO/Al_2O_3$ Catalyst. *Catalysts* **2017**, *7*, 332. [CrossRef]

8. Daza, Y.A.; Kuhn, J.N. CO_2 conversion by reverse water gas shift catalysis: Comparison of catalysts, mechanisms and their consequences for CO_2 conversion to liquid fuels. *RSC Adv.* **2016**, *6*, 49675–49691. [CrossRef]
9. Zhang, L.; Chen, L.; Xia, S.; Wang, C.; Sun, F. Entropy generation minimization for the reverse water gas shift (RWGS) reactors. *Entropy* **2018**, *20*, 415. [CrossRef]
10. Liang, B.; Duan, H.; Su, X.; Chen, X.; Huang, Y.; Chen, X.; Delgado, J.J.; Zhang, T. Promoting role of potassium in the reverse water gas shift reaction on Pt/mullite catalyst. *Catal. Today* **2017**, *281*, 319–326. [CrossRef]
11. Álvarez Galván, C.; Schumann, J.; Behrens, M.; Fierro, J.L.G.; Schlögl, R.; Frei, E. Reverse water-gas shift reaction at the Cu/ZnO interface: Influence of the cu/zn ratio on structure-activity correlations. *Appl. Catal. B* **2016**, *195*, 104–111. [CrossRef]
12. Liu, Y.; Liu, D. Study of bimetallic Cu–Ni/γ-Al_2O_3 catalysts for carbon dioxide hydrogenation. *Int. J. Hydrogen Energy* **1999**, *24*, 351–354. [CrossRef]
13. Nagai, M.; Kurakami, T. Reverse water gas shift reaction over molybdenum carbide. *J. Chem. Eng. Jpn.* **2005**, *38*, 807–812. [CrossRef]
14. Bligaard, T.; Nørskov, J.K.; Dahl, S.; Matthiesen, J.; Christensen, C.H.; Sehested, J. The brønsted–evans–polanyi relation and the volcano curve in heterogeneous catalysis. *J. Catal.* **2004**, *224*, 206–217. [CrossRef]
15. Peña, D.; Cognigni, A.; Neumayer, T.; van Beek, W.; Jones, D.S.; Quijada, M.; Rønning, M. Identification of carbon species on iron-based catalysts during fischer-tropsch synthesis. *Appl. Catal. A* **2018**, *554*, 10–23. [CrossRef]
16. Wenzel, M.; Aditya Dharanipragada, N.V.R.; Galvita, V.V.; Poelman, H.; Marin, G.B.; Rihko-Struckmann, L.; Sundmacher, K. Co production from CO_2 via reverse water–gas shift reaction performed in a chemical looping mode: Kinetics on modified iron oxide. *J. CO_2 Util.* **2017**, *17*, 60–68. [CrossRef]
17. Chen, X.; Su, X.; Duan, H.; Liang, B.; Huang, Y.; Zhang, T. Catalytic performance of the Pt/TiO_2 catalysts in reverse water gas shift reaction: Controlled product selectivity and a mechanism study. *Catal. Today* **2017**, *281*, 312–318. [CrossRef]
18. Wang, L.; Zhang, S.; Liu, Y. Reverse water gas shift reaction over co-precipitated Ni-CeO_2 catalysts. *J. Rare Earths* **2008**, *26*, 66–70. [CrossRef]
19. Kharaji, A.G.; Shariati, A.; Takassi, M.A. A novel γ-Alumina supported Fe-Mo bimetallic catalyst for reverse water gas shift reaction. *Chin. J. Chem. Eng.* **2013**, *21*, 1007–1014. [CrossRef]
20. Jurković, D.L.; Pohar, A.; Dasireddy, V.D.B.C.; Likozar, B. Effect of copper-based catalyst support on reverse water-gas shift reaction (RWGS) activity for CO_2 reduction. *Chem. Eng. Technol.* **2017**, *40*, 973–980. [CrossRef]
21. Santos, J.L.; Bobadilla, L.F.; Centeno, M.A.; Odriozola, J.A. Operando DRIFTS-MS Study of WGS and rWGS Reaction on Biochar-Based Pt Catalysts: The Promotional Effect of Na. *C* **2018**, *4*, 47. [CrossRef]
22. Sai Prasad, P.S.; Bae, J.W.; Jun, K.-W.; Lee, K.-W. Fischer–tropsch synthesis by carbon dioxide hydrogenation on fe-based catalysts. *Catal. Surv. Asia* **2008**, *12*, 170–183. [CrossRef]
23. Visconti, C.G.; Martinelli, M.; Falbo, L.; Infantes-Molina, A.; Lietti, L.; Forzatti, P.; Iaquaniello, G.; Palo, E.; Picutti, B.; Brignoli, F. CO_2 hydrogenation to lower olefins on a high surface area K-promoted bulk fe-catalyst. *Appl. Catal. B* **2017**, *200*, 530–542. [CrossRef]
24. Park, J.C.; Yeo, S.C.; Chun, D.H.; Lim, J.T.; Yang, J.-I.; Lee, H.-T.; Hong, S.; Lee, H.M.; Kim, C.S.; Jung, H. Highly activated K-doped iron carbide nanocatalysts designed by computational simulation for fischer–tropsch synthesis. *J. Mater. Chem. A* **2014**, *2*, 14371–14379. [CrossRef]
25. Loiland, J.A.; Wulfers, M.J.; Marinkovic, N.S.; Lobo, R.F. Fe/γ-Al_2O_3 and Fe-K/γ-Al_2O_3 as reverse water-gas shift catalysts. *Catal. Sci. Technol.* **2016**, *6*, 5267–5279. [CrossRef]
26. Bobadilla, L.F.; Riesco-García, J.M.; Penelás-Pérez, G.; Urakawa, A. Enabling continuous capture and catalytic conversion of flue gas CO_2 to syngas in one process. *J. CO_2 Util.* **2016**, *14*, 106–111. [CrossRef]
27. Pastor-Pérez, L.; Baibars, F.; le Saché, E.; Arellano-García, H.; Gu, S.; Reina, T.R. CO_2 valorisation via reverse water-gas shift reaction using advanced Cs doped Fe-Cu/Al_2O_3 catalysts. *J. CO_2 Util.* **2017**, *21*, 423–428. [CrossRef]
28. Yang, X.; Su, X.; Chen, X.; Duan, H.; Liang, B.; Liu, Q.; Liu, X.; Ren, Y.; Huang, Y.; Zhang, T. Promotion effects of potassium on the activity and selectivity of Pt/zeolite catalysts for reverse water gas shift reaction. *Appl. Catal. B* **2017**, *216*, 95–105. [CrossRef]

29. Ahlers, S.J.; Pohl, M.-M.; Radnik, J.; Linke, D.; Kondratenko, E.V. Catalytic role and location of cs promoter in Cs–Au/TiO_2 catalysts for propanol synthesis from CO_2, C_2H_4 and H_2. *Appl. Catal. B* **2015**, *176–177*, 570–577. [CrossRef]
30. Ali, S.; Mohd Zabidi, N.A.; Subbarao, D. Correlation between fischer-tropsch catalytic activity and composition of catalysts. *Chem. Cent. J.* **2011**, *5*, 68. [CrossRef]
31. Yang, L.; Pastor-Pérez, L.; Gu, S.; Sepúlveda-Escribano, A.; Reina, T.R. Highly efficient Ni/CeO_2-Al_2O_3 catalysts for CO_2 upgrading via reverse water-gas shift: Effect of selected transition metal promoters. *Appl. Catal. B* **2018**, *232*, 464–471. [CrossRef]
32. Nist X-ray Photoelectron Spectroscopy Database. Available online: https://srdata.nist.gov/xps/Default.aspx (accessed on 8 November 2018).
33. Park, S.-W.; Joo, O.-S.; Jung, K.-D.; Kim, H.; Han, S.-H. Development of ZnO/Al_2O_3 catalyst for reverse-water-gas-shift reaction of camere (carbon dioxide hydrogenation to form methanol via a reverse-water-gas-shift reaction) process. *Appl. Catal. A* **2001**, *211*, 81–90. [CrossRef]
34. Aljishi, A.; Veilleux, G.; Lalinde, J.A.H.; Kopyscinski, J. The effect of synthesis parameters on ordered mesoporous nickel alumina catalyst for CO_2 methanation. *Appl. Catal. A* **2018**, *549*, 263–272. [CrossRef]
35. Zhang, C.; Zhao, G.; Liu, K.; Yang, Y.; Xiang, H.; Li, Y. Adsorption and reaction of CO and hydrogen on iron-based fischer–tropsch synthesis catalysts. *J. Mol. Catal. A Chem.* **2010**, *328*, 35–43. [CrossRef]
36. Ghodoosi, F.; Khosravi-Nikou, M.R.; Shariati, A. Mathematical modeling of reverse water-gas shift reaction in a fixed-bed reactor. *Chem. Eng. Technol.* **2017**, *40*, 598–607. [CrossRef]